Editors' Suggestion | Featured in Physics

Laughlin's Topological Charge Pump in an Atomic Hall Cylinder

Aurélien Fabre, Jean-Baptiste Bouhiron, Tanish Satoor, Raphael Lopes, and Sylvain Nascimbene*
Laboratoire Kastler Brossel, Collège de France, CNRS, ENS-PSL University, Sorbonne Université, 11 Place Marcelin Berthelot, 75005 Paris, France

(Received 17 November 2021; accepted 25 February 2022; published 25 April 2022)

The quantum Hall effect occurring in two-dimensional electron gases was first explained by Laughlin, who developed a thought experiment that laid the groundwork for our understanding of topological quantum matter. His proposal is based on a quantum Hall cylinder periodically driven by an axial magnetic field, resulting in the quantized motion of electrons. We realize this milestone experiment with an ultracold gas of dysprosium atoms, the cyclic dimension being encoded in the electronic spin and the axial field controlled by the phases of laser-induced spin-orbit couplings. Our experiment provides a straightforward manifestation of the nontrivial topology of quantum Hall insulators, and could be generalized to strongly correlated topological systems.

DOI: 10.1103/PhysRevLett.128.173202

The quantization of Hall conductance observed in two-dimensional electronic systems subjected to a perpendicular magnetic field [1] is intimately linked to the nontrivial topology of Bloch bands [2] and the occurrence of chiral edge modes protected from backscattering [3]. The first step in its understanding was provided by Laughlin, who gave an elegant argument by considering a Hall system in a cylindrical geometry (Fig. 1) [4]. Besides the radial magnetic field $\mathbf{B}_\perp$ yielding the Hall effect, this geometry authorizes an axial field $\mathbf{B}_\parallel$, which does not pierce the surface but threads the cylinder with a flux $\Phi_\parallel$. Varying the flux $\Phi_\parallel$ controls a quantized electronic motion along the tube, which is directly linked to the underlying band topology. Such quantization of transport was later generalized by Thouless to any physical system subjected to a slow periodic deformation [5], as implemented in electronic quantum dots [6,7], photonic waveguides [8], and ultracold atomic gases [9,10].

So far, the topology of magnetic Bloch bands has been revealed in planar systems only, by measuring the quantization of transverse response [1,11–13] or observing chiral ballistic edge modes [14–16]. The realization of Laughlin's pump experiment requires engineering periodic boundary conditions, which is challenging when using genuine spatial dimensions. The concept of a synthetic dimension encoded in an internal degree of freedom provides an alternative method for the generation of gauge fields [17]. Synthetic dimensions were first implemented with open boundary conditions, leading to the observation of chiral edge modes [18,19]. More recently, synthetic Hall cylinders were engineered using several spin states coupled in a cyclic manner [20–22]. Nevertheless, the realization of Laughlin's topological charge pump was not realized yet, due to the absence of control over an axial magnetic field $\mathbf{B}_\parallel$.

In this Letter, we use an ultracold gas of ^{162}Dy atoms to engineer a Hall cylinder whose azimuthal coordinate is encoded in the electronic spin $J = 8$ [23]. We manipulate the spin using coherent optical transitions, such that a triplet of internal states coupled in a cyclic manner emerges at low energy, leading to an effective cylindrical geometry [24]. The exchange of momentum between light and atoms leads to a spin-orbit coupling that mimics a radial magnetic field $\mathbf{B}_\perp$ [25]. The phases of the laser electric fields also control an effective axial field $\mathbf{B}_\parallel$, which is the crucial ingredient to implement Laughlin's thought experiment and reveal the underlying topology. The topological character of the

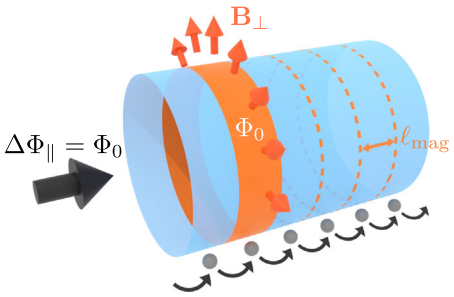

FIG. 1. Laughlin's thought experiment. Scheme of a two-dimensional electronic system in a cylindrical geometry, with a radial magnetic field $\mathbf{B}_\perp$ producing a quantum Hall effect. The orange area, pierced by one magnetic flux quantum Φ_0, defines the length ℓ_{mag} of the magnetic unit cell—each cell being filled with one electron in a quantum Hall insulator. Laughlin's thought experiment consists of performing an adiabatic cycle by threading one flux quantum $\Delta\Phi_\parallel = \Phi_0$ through the cylinder. The cycle shifts electron occupations by one unit cell, such that a single electron is pumped from one edge to the other, or equivalently the center-of-mass position is displaced by ℓ_{mag}.

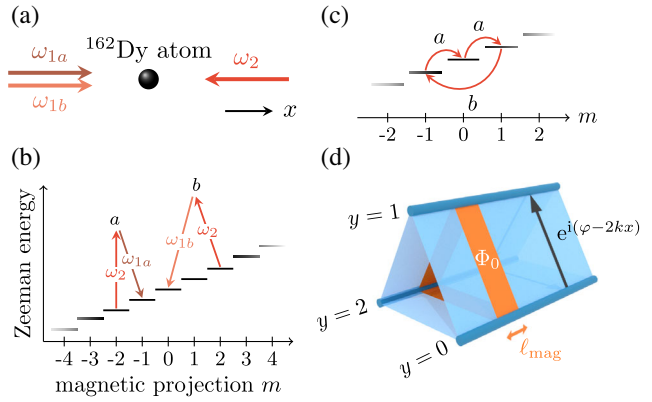

FIG. 2. Emerging quantum Hall cylinder. (a) Sketch of the laser configuration involving two beams counterpropagating along x and sent on a thermal sample of dysprosium atoms—one beam having two frequency components. (b) Scheme of the two-photon optical transitions resonantly driving first- and second-order spin transitions, labeled a and b, respectively. (c) Representation of a nontrivial 3-cycle between magnetic sublevels induced by the light couplings. (d) Scheme of the Hall cylinder dynamics emerging at low energy, involving three spin states $|y\rangle$ (with $y = 0$, 1, and 2). The hopping amplitudes have a complex phase $\varphi - 2kx$, where $2\hbar k$ plays the role of a radial magnetic field $B_\perp$ and φ is linked to an axial field $B_\parallel$. The orange area, of length $\ell_{\rm mag} = \lambda/6$ is threaded by one unit of magnetic flux quantum Φ_0.

ground Bloch band manifests as well in a complementary pump experiment driven by Bloch oscillations.

In our experimental protocol, we apply a magnetic field in order to lift the degeneracy between the magnetic sublevels m (with $-J \le m \le J$ and integer m). Spin transitions of first and second order, i.e., $\Delta m = \pm 1$ and ± 2, are induced by resonant two-photon optical transitions, using a pair of laser beams counterpropagating along x [Fig. 2(a)] [26]. The configuration of laser frequencies is chosen such that the atoms undergo a momentum kick $-2\hbar k$ upon either resonant process $m \to m+1$ or $m \to m-2$, shown in Fig. 2(b). Here, $k = 2\pi/\lambda$ is the photon momentum for the laser wavelength $\lambda = 626.1$ nm. The resulting spin-orbit coupling breaks continuous translation symmetry, but conserves the quasimomentum $q = Mv_x/\hbar + 2km (\mathrm{mod}\ 6k)$, defined over the magnetic Brillouin zone $-3k \le q < 3k$, where M and v_x are the atomic mass and velocity. The atom dynamics is described by the Hamiltonian

$$H = \frac{1}{2} M v_x^2 + V, \tag{1}$$

$$V = -\mathcal{T}_y e^{-2ikx} + \mathrm{H.c.}, \quad \mathcal{T}_y = t_a e^{i\varphi_a} \frac{J_+}{J} + t_b e^{i\varphi_b} \frac{J_-^2}{J^2}, \tag{2}$$

where J_+ and J_- are the spin ladder operators, and $t_a, t_b > 0$ are the strengths of the first- and second-order transitions. The phase difference $\varphi_a - \varphi_b$ can be gauged away using a suitable spin rotation, such that we retain hereafter a single phase $\varphi \equiv \varphi_a = \varphi_b$.

The combination of the two types of transitions induces nontrivial 3-cycles $m \to m+1 \to m+2 \to m$ [Fig. 2(b)], with chiral dynamics in the cyclic variable $y = m (\mathrm{mod}\ 3)$—each step increasing y by one unit. As explained in a previous theoretical work [24] and in the Supplemental Material [26], this dynamics leads to the emergence at low energy of a closed subsystem of dimension 3, spanned by three spin states $|y\rangle$, with $y = 0$, 1, 2 and where $|y\rangle$ expands on projection states $|m\rangle$ with $m = y (\mathrm{mod}\ 3)$ only. The $|y\rangle$ states are obtained by linear combinations of three coherent spin states oriented along equatorial directions of azimuthal angles $\phi = \varphi + \{0, 2\pi/3, 4\pi/3\}$. Hence, they only involve magnetic projections m around 0, with a rms width $\Delta m = \sqrt{J/2} = 2$. The $|y\rangle$ states will be interpreted in the following as position eigenstates along a cyclic synthetic dimension of length $Y = 3$. The operator $\mathcal{T}_y$ involved in the spin coupling [Eq. (2)] then acts as a translation $\mathcal{T}_y|y\rangle = t|y+1\rangle$, with a hopping amplitude $t = t_a + t_b$. The low-energy spin dynamics is described by the effective potential

$$V_{\rm eff} = -t \sum_{y=0}^{2} (e^{i(\varphi - 2kx)} |y+1\rangle\langle y| + \mathrm{hc}). \tag{3}$$

Together with the kinetic energy $\frac{1}{2} M v_x^2$, it describes the motion of a particle on a cylinder discretized along its circumference [see Fig. 2(c)]. The complex phase $2kx$ mimics the Aharonov-Bohm phase associated with a radial magnetic field $B_\perp = 2\hbar k$ (assuming a particle charge $q = -1$). It defines a magnetic length $\ell_{\rm mag} = \lambda/6$, such that the magnetic flux $\Phi_\perp = \ell_{\rm mag} Y B_\perp$ through a portion of cylinder of length $\ell_{\rm mag}$ equals the flux quantum $\Phi_0 = h/|q|$.

Experimentally, we use a gas of about 4×10^4 atoms, initially prepared at a temperature $T = 0.54(3)$ μK, such that the thermal momentum width $\sigma_q \simeq 1.3k$ is much smaller than the Brillouin zone extent $6k$, and interaction effects can be neglected on the time scale of our experiments. The atoms are adiabatically loaded in the ground Bloch band with $t_a = 11.5(3) E_r$ and $t_b = 7.1(2) E_r$, by ramping the light coupling parameters. Here, $E_r = \hbar^2 k^2/(2M)$ is the single-photon recoil energy. The mean quasimomentum $\langle q \rangle$ is controlled by applying a weak force F_x after the loading (see the Supplemental Material [26]). We simultaneously probe the distribution of velocity v_x and spin projection m. For this, we abruptly switch off the light couplings and ramp up a magnetic field gradient that spatially separates the different magnetic sublevels along z. The velocity distribution is obtained from the density

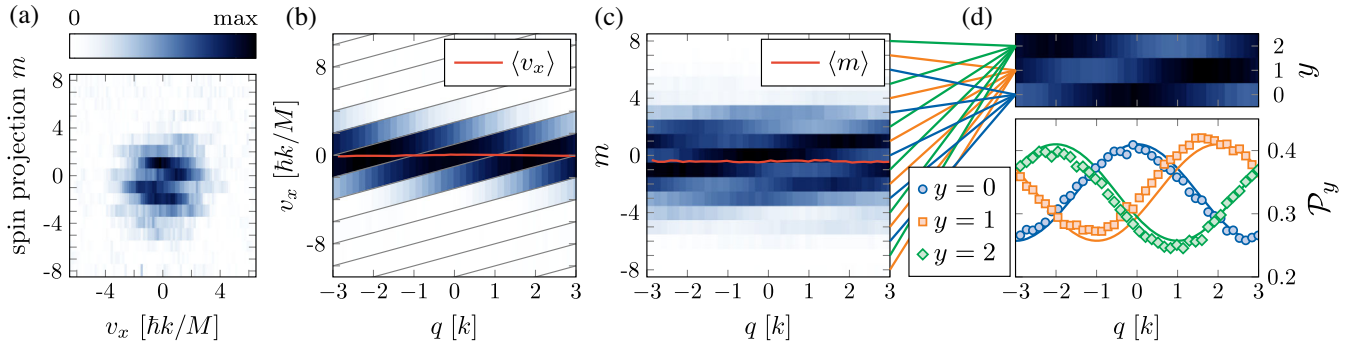

FIG. 3. Ground band characterization. (a) Spin-resolved velocity distribution measured for a gas of mean quasimomentum $\langle q \rangle \simeq 2k$. (b) Distribution of discrete velocity components $v_x = \hbar(q + 2kp)/M$ (with integer p) for states of quasimomentum q. The red line shows the mean velocity $\langle v_x \rangle$. (c) Spin projection probabilities Π_m measured as a function of q. The red line stands for the mean spin projection $\langle m \rangle$. (d) Probabilities $\mathcal{P}_y$ of projection on $y = m (\mathrm{mod}\ 3)$. The blue circles, orange squares, and green diamonds correspond to $y = 0$, 1, and 2, respectively. Statistical error bars, computed from a bootstrap random sampling analysis, are smaller than the symbols. The lines are calculated from the expected band structure.

profile along x measured after a 2.3 ms expansion. A typical spin-resolved velocity distribution is shown in Fig. 3(a).

The velocity distribution, plotted in Fig. 3(b) as a function of q, exhibits a period $2k$, similar to the case of a simple $\lambda/2$-lattice. The mean velocity $\langle v_x \rangle$, shown as a red line, remains close to zero. Since it is linked to the slope of the ground-band energy $\partial_q E_0(q) = \hbar \langle v_x \rangle$, this shows that the band is quasiflat. In fact, the band's flatness is protected from pertubations, such as external magnetic field fluctuations, by the zero net magnetization of the $|y\rangle$ spin states—a similar effect has been used in another implementation of a Hall cylinder using dynamical decoupling techniques [22].

The probabilities Π_m of projection on each sublevel m reveal a longer periodicity $6k$ [Fig. 3(c)], corresponding to the full extent of the magnetic Brillouin zone. It experimentally confirms the spatial separation of magnetic orbitals $\ell_{\mathrm{mag}} = 2\pi/(6k) = \lambda/6$ introduced above. The Π_m measurements also give access to the probabilities $\mathcal{P}_y$ of projection on the synthetic coordinate y, by summing the Π_m's with $m = y (\mathrm{mod}\ 3)$ [Fig. 3(d)]. The q variation of these distributions reveals a chirality typical of the Hall effect: when increasing the momentum by $2k$, the $\mathcal{P}_y$ distributions cycle along the synthetic dimension in a directional manner, as $\mathcal{P}_y \to \mathcal{P}_{y+1}$ [30,31]. We stress that such a drift does not occur on the mean spin projection $\langle m \rangle$, which remains close to zero [red line in Fig. 3(c)].

The adiabatic y drift occurring during Bloch oscillations provides a first insight into the topological character of the lowest energy band—similar to the quantized flow of Wannier function charge centers in Chern insulators [32]. To quantify this drift, we cannot rely on the mean y position, which is ill defined for a cyclic dimension [33]. Instead, it is reconstructed by integrating the anomalous velocity $\langle v_y \rangle \equiv \partial_\varphi H/\hbar$ induced by the force F_x driving the Bloch oscillation. For this purpose, we conduct a separate experiment, in which we suddenly switch off the force F_x, such that the center of mass undergoes a cyclotron oscillation, with the x and y velocities oscillating in quadrature. More precisely, the rate of change of the x velocity gives access to the y velocity, via the exact relation

$$\partial_t \langle v_x \rangle = \frac{i}{\hbar}[H, v_x] = -\frac{2\hbar k}{M}\langle v_y \rangle.$$

Hence, the velocity $\langle v_y \rangle$ induced by the force F_x is given by the initial slope of $\langle v_x \rangle$ [Fig. 4(b)].

The center-of-mass drift $\langle \Delta y \rangle$, obtained upon integration of $\langle v_y \rangle$ is shown in Fig. 4(a). We find that it varies linearly with the quasimomentum variation Δq [Fig. 4(a)], such that the drift per Bloch oscillation cycle reads

$$\frac{\langle \Delta y \rangle}{Y} = 0.97(5), \tag{4}$$

consistent with a unit winding around the cylinder of circumference Y [26]. The rotation along y occurring over a Bloch oscillation cycle is thus quantized, providing a first manifestation of the nontrivial band topology.

We now characterize the global band topology by implementing Laughlin's charge pump experiment, and extend the protocol to reveal the local geometrical properties. To simulate the axial magnetic field used to drive the pump, we interpret the complex phase φ involved in the y hoppings [see Eq. (3)] as the Peierls phase associated with the field $\mathbf{B}_\parallel$ threading the cylinder with a flux

$$\Phi_\parallel = \frac{3\varphi}{2\pi}\Phi_0. \tag{5}$$

We vary $\Phi_\parallel$ by adjusting the phase difference φ between the laser electric fields involved in the spin transitions using acousto-optic modulators.

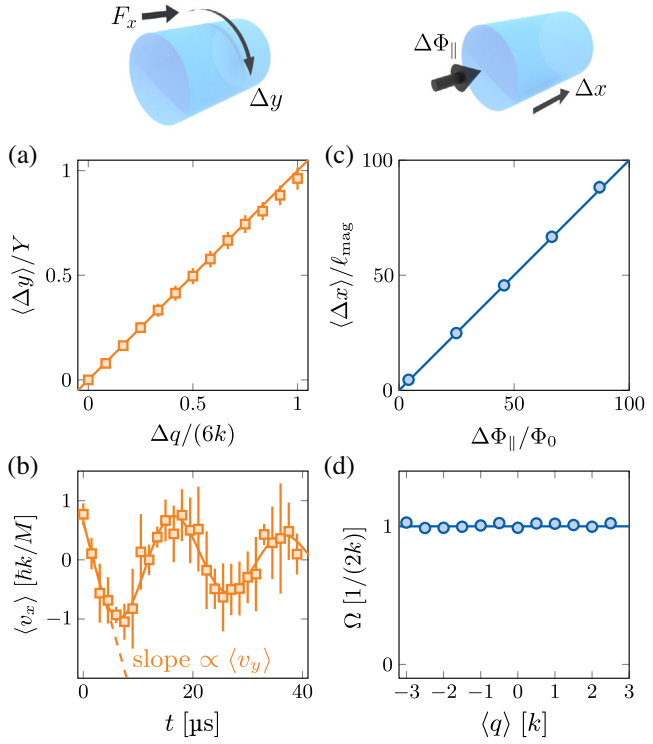

FIG. 4. Topological charge pumps. (a) Center-of-mass displacement $\langle\Delta y\rangle$ as a function of the quasimomentum shift Δq induced by a force F_x (orange squares), together with a linear fit (orange line). (b) Evolution of the mean velocity $\langle v_x\rangle$ immediately after switching off the force F_x (orange squares), fitted with a damped sine (solid line). The velocity $\langle v_y\rangle$ is obtained from the initial slope of the fit (dashed line). (c) Displacement of the center of mass $\langle\Delta x\rangle$ induced by an axial magnetic flux $\Phi_\parallel$ and averaged over the magnetic Brillouin zone (blue circles). The blue line is a linear fit. (d) Berry curvature Ω measured as a function of the mean quasimomentum $\langle q\rangle$ (blue circles). The solid line is the expected Berry curvature, which is not distinguishable from the constant value $\Omega(q) = 1/(2k)$.

We drive the pump by slowly ramping the phase φ, and measure the induced shift of the center of mass along the real dimension x. The experiment is performed for various values of the quasimomentum $\langle q\rangle$ uniformly spanning the magnetic Brillouin zone. The q-averaged drift, shown in Fig. 4(c), is consistent with a linear variation

$$\frac{\langle\Delta x\rangle}{\ell_{\mathrm{mag}}} = \mathcal{C}\frac{\Phi_\parallel}{\Phi_0}, \qquad \mathcal{C} = 1.00(4),$$

in agreement with the expected quantization of transport by the Chern number $\mathcal{C} = 1$. The pump adiabaticity is checked by repeating the experiment for various speeds of the flux ramp, and measuring identical responses for slow enough ramps [26].

Our experiments also give access to the anomalous drift of individual momentum states $\Delta x = \Omega(q)\varphi$, proportional to the Berry curvature $\Omega(q)$ that quantifies the local geometrical properties of quantum states [34]. As shown in Fig. 4(d), the measured Berry curvature is flat within error bars, consistent with theory, which predicts $\Omega(q) = 1/(2k)$ with negligible q variation. The flatness of the Berry curvature is a consequence of the continuous translation symmetry along x, making our system similar to continuous two-dimensional systems with flat Landau levels. In contrast, discrete lattice systems, such as Hofsdtater and Haldane models [35,36], or previous implementations of synthetic Hall cylinders [20–22], exhibit dispersive bands with inhomogeneous Berry curvatures.

We have shown that implementing a quantum Hall cylinder gives direct access to the underlying topology of Bloch bands. Our realization of Laughlin's pump protocol could be generalized to interacting atomic systems, which are expected to form strongly correlated topological states of matter at low temperature. In particular, at fractional fillings, one expects the occurrence of charge density waves as one-dimensional precursors of two-dimensional fractional quantum Hall states [37]. The pumped charge would then be quantized to a rational value, revealing the charge fractionalization of elementary excitations [38].

We thank Jean Dalibard for insightful discussions and careful reading of the manuscript, and Thomas Chalopin for discussions at an early stage of this work. This work is supported by the European Union (Grant No. TOPODY 756722 from the European Research Council).

*sylvain.nascimbene@lkb.ens.fr

[1] K. v. Klitzing, G. Dorda, and M. Pepper, New Method for High-Accuracy Determination of the Fine-Structure Constant Based on Quantized Hall Resistance, Phys. Rev. Lett. **45**, 494 (1980).
[2] D. J. Thouless, M. Kohmoto, M. P. Nightingale, and M. den Nijs, Quantized Hall Conductance in a Two-Dimensional Periodic Potential, Phys. Rev. Lett. **49**, 405 (1982).
[3] B. I. Halperin, Quantized Hall conductance, current-carrying edge states, and the existence of extended states in a two-dimensional disordered potential, Phys. Rev. B **25**, 2185 (1982).
[4] R. B. Laughlin, Quantized Hall conductivity in two dimensions, Phys. Rev. B **23**, 5632 (1981).
[5] D. J. Thouless, Quantization of particle transport, Phys. Rev. B **27**, 6083 (1983).
[6] M. Switkes, C. M. Marcus, K. Campman, and A. C. Gossard, An adiabatic quantum electron pump, Science **283**, 1905 (1999).
[7] S. K. Watson, R. M. Potok, C. M. Marcus, and V. Umansky, Experimental Realization of a Quantum Spin Pump, Phys. Rev. Lett. **91**, 258301 (2003).
[8] Y. E. Kraus, Y. Lahini, Z. Ringel, M. Verbin, and O. Zilberberg, Topological States and Adiabatic Pumping in Quasicrystals, Phys. Rev. Lett. **109**, 106402 (2012).

[9] M. Lohse, C. Schweizer, O. Zilberberg, M. Aidelsburger, and I. Bloch, A Thouless quantum pump with ultracold bosonic atoms in an optical superlattice, Nat. Phys. **12**, 350 (2016).
[10] S. Nakajima, T. Tomita, S. Taie, T. Ichinose, H. Ozawa, L. Wang, M. Troyer, and Y. Takahashi, Topological Thouless pumping of ultracold fermions, Nat. Phys. **12**, 296 (2016).
[11] C. R. Dean, L. Wang, P. Maher, C. Forsythe, F. Ghahari, Y. Gao, J. Katoch, M. Ishigami, P. Moon, M. Koshino, T. Taniguchi, K. Watanabe, K. L. Shepard, J. Hone, and P. Kim, Hofstadter's butterfly and the fractal quantum Hall effect in moiré superlattices, Nature (London) **497**, 598 (2013).
[12] L. A. Ponomarenko, R. V. Gorbachev, G. L. Yu, D. C. Elias, R. Jalil, A. A. Patel, A. Mishchenko, A. S. Mayorov, C. R. Woods, J. R. Wallbank, M. Mucha-Kruczynski, B. A. Piot, M. Potemski, I. V. Grigorieva, K. S. Novoselov, F. Guinea, V. I. Fal'ko, and A. K. Geim, Cloning of Dirac fermions in graphene superlattices, Nature (London) **497**, 594 (2013).
[13] M. Aidelsburger, M. Lohse, C. Schweizer, M. Atala, J. T. Barreiro, S. Nascimbene, N. Cooper, I. Bloch, and N. Goldman, Measuring the Chern number of Hofstadter bands with ultracold bosonic atoms, Nat. Phys. **11**, 162 (2015).
[14] Z. Wang, Y. Chong, J. D. Joannopoulos, and M. Soljačić, Observation of unidirectional backscattering-immune topological electromagnetic states, Nature (London) **461**, 772 (2009).
[15] M. Hafezi, S. Mittal, J. Fan, A. Migdall, and J. Taylor, Imaging topological edge states in silicon photonics, Nat. Photonics **7**, 1001 (2013).
[16] M. C. Rechtsman, J. M. Zeuner, Y. Plotnik, Y. Lumer, D. Podolsky, F. Dreisow, S. Nolte, M. Segev, and A. Szameit, Photonic Floquet topological insulators, Nature (London) **496**, 196 (2013).
[17] A. Celi, P. Massignan, J. Ruseckas, N. Goldman, I. B. Spielman, G. Juzeliūnas, and M. Lewenstein, Synthetic Gauge Fields in Synthetic Dimensions, Phys. Rev. Lett. **112**, 043001 (2014).
[18] M. Mancini, G. Pagano, G. Cappellini, L. Livi, M. Rider, J. Catani, C. Sias, P. Zoller, M. Inguscio, M. Dalmonte, and L. Fallani, Observation of chiral edge states with neutral fermions in synthetic Hall ribbons, Science **349**, 1510 (2015).
[19] B. K. Stuhl, H.-I. Lu, L. M. Aycock, D. Genkina, and I. B. Spielman, Visualizing edge states with an atomic Bose gas in the quantum Hall regime, Science **349**, 1514 (2015).
[20] J. H. Han, J. H. Kang, and Y. Shin, Band Gap Closing in a Synthetic Hall Tube of Neutral Fermions, Phys. Rev. Lett. **122**, 065303 (2019).
[21] C.-H. Li, Y. Yan, S. Choudhury, D. B. Blasing, Q. Zhou, and Y. P. Chen, A Bose-Einstein condensate on a synthetic Hall cylinder, PRX Quantum **3**, 010316 (2022).
[22] Q.-Y. Liang, D. Trypogeorgos, A. Valdés-Curiel, J. Tao, M. Zhao, and I. B. Spielman, Coherence and decoherence in the Harper-Hofstadter model, Phys. Rev. Research **3**, 023058 (2021).
[23] T. Chalopin, T. Satoor, A. Evrard, V. Makhalov, J. Dalibard, R. Lopes, and S. Nascimbene, Probing chiral edge dynamics and bulk topology of a synthetic Hall system, Nat. Phys. **16**, 1017 (2020).
[24] A. Fabre, J.-B. Bouhiron, T. Satoor, R. Lopes, and S. Nascimbene, Simulating two-dimensional dynamics within a large-size atomic spin, Phys. Rev. A **105**, 013301 (2022).
[25] J. Dalibard, F. Gerbier, G. Juzeliūnas, and P. Öhberg, Colloquium: Artificial gauge potentials for neutral atoms, Rev. Mod. Phys. **83**, 1523 (2011).
[26] See Supplemental Material at http://link.aps.org/supplemental/10.1103/PhysRevLett.128.173202 for details on the experimental protocol, additional information on the derivation of the three-state model and on the link between adiabatic pumps and band topology, a study of the pump adiabaticity and measurements of low-energy excitations, which includes Refs. [27–29].
[27] C. Cohen-Tannoudji and J. Dupont-Roc, Experimental study of Zeeman light shifts in weak magnetic fields, Phys. Rev. A **5**, 968 (1972).
[28] F. T. Arecchi, E. Courtens, R. Gilmore, and H. Thomas, Atomic coherent states in quantum optics, Phys. Rev. A **6**, 2211 (1972).
[29] X.-W. Luo, J. Zhang, and C. Zhang, Tunable flux through a synthetic Hall tube of neutral fermions, Phys. Rev. A **102**, 063327 (2020).
[30] Y. Yan, S.-L. Zhang, S. Choudhury, and Q. Zhou, Emergent Periodic and Quasiperiodic Lattices on Surfaces of Synthetic Hall Tori and Synthetic Hall Cylinders, Phys. Rev. Lett. **123**, 260405 (2019).
[31] R. P. Anderson, D. Trypogeorgos, A. Valdés-Curiel, Q.-Y. Liang, J. Tao, M. Zhao, T. Andrijauskas, G. Juzeliūnas, and I. B. Spielman, Realization of a deeply subwavelength adiabatic optical lattice, Phys. Rev. Research **2**, 013149 (2020).
[32] M. Taherinejad, K. F. Garrity, and D. Vanderbilt, Wannier center sheets in topological insulators, Phys. Rev. B **89**, 115102 (2014).
[33] R. Lynch, The quantum phase problem: A critical review, Phys. Rep. **256**, 367 (1995).
[34] H.-I. Lu, M. Schemmer, L. M. Aycock, D. Genkina, S. Sugawa, and I. B. Spielman, Geometrical Pumping with a Bose-Einstein Condensate, Phys. Rev. Lett. **116**, 200402 (2016).
[35] D. R. Hofstadter, Energy levels and wave functions of Bloch electrons in rational and irrational magnetic fields, Phys. Rev. B **14**, 2239 (1976).
[36] F. D. M. Haldane, Model for a Quantum Hall Effect without Landau Levels: Condensed-Matter Realization of the "Parity Anomaly", Phys. Rev. Lett. **61**, 2015 (1988).
[37] R. Tao and D. J. Thouless, Fractional quantization of Hall conductance, Phys. Rev. B **28**, 1142 (1983).
[38] R. B. Laughlin, Nobel lecture: Fractional quantization, Rev. Mod. Phys. **71**, 863 (1999).